IMAM KHOMEINI INTERNATIONAL UNIVERSITY
Vol. 6, No. 1, Spring 2021, pp. 41-52
دوره ششم، شماره ۱، بهار ۱۴۰۰، صفحه ۴۱ تا ۵۲
نشریه مهندسی منابع معدنی
Journal of Mineral Resources Engineering (JMRE)
DOI: 10.30479/jmre.2019.10985.1283
Research Paper

Investigating the Effects of Rock Failure Mechanism on its Bearing Capacity Using the Three Dimensional Particle Flow Code (PFC3D)

Sepehri S.[1], Shirinabadi R.[2*], Hosseini Alae N.[2], Moosavi E.[2], Bangian A.[2]

1- Ph.D Student, Dept. of Mining Engineering, South Tehran Branch, Islamic Azad University, Tehran, Iran
2- Assistant Professor, Dept. of Mining Engineering, South Tehran Branch, Islamic Azad University, Tehran, Iran

(Received: 15 Jun. 2019, Accepted: 07 Sep. 2019)

Abstract

One of the most important issues in geotechnical studies is bearing capacity. It is also defined as the resistance when the maximum pressure is exerted from the footing to the foundation without creating shear failure therein. Since earing capacity is highly correlated with the stability of surface and subsurface structures, researchers have become interested in this subject. The area and geometry impacts on the footing are considered as the two important issues in this regard. In this research, a numerical model based on particle flow code was used in PFC3D software. To do experiments in numerical models, two triple-facet footings were utilized in square, rectangular and circular geometric shapes. Furthermore, these footings held a total area of 64 cm^2 and other series included a full area of 49 cm^2. In the modeling, the mechanical properties of granite were put into practice and the results of the numerical tests were scrutinized, as well. As a result, it was ascertained that the bearing capacity depends on both the footing geometry and the footing area.

Keywords

Bearing capacity, Footing geometry, Foundation, Shear failure mechanism, Particle flow code.

Corresponding Author, Email: r_shirinabadi@azad.ac.ir

1- INTRODUCTION

Many geo-mechanical problems involved in the fields of mining, civil, petroleum and environmental engineering are very complicated. The experimental, empirical, and analytical solutions are not efficient enough to satisfy the suitable and sound design status of many engineering problems which are related to rock engineering and geo-mechanics. Therefore, several sophisticated numerical methods such as finite element method (FEM), finite difference method (FDM) and boundary element method (BEM) have been developed to improve the modern engineering needs for the design of huge foundations and structures. For example, the continuum based higher order displacement discontinuity method (HODDM), which is a version of the indirect BEM, has been widely applied to remove many rock mechanics problems dealt with rock fragmentations, rock cuttings, hydraulic fracturing and many other related problems [1-7]. On the other hand, the dis-continuum based finite difference method, known as (DEM), has been extensively employed to elucidate problems related to the discontinuous jointed rock mass in geo-mechanics [8-10]. Currently, the tensile and shear failure mechanism of rocks and concretes as well as some hydraulic fracturing related problems have been studied by the improved two- and three-dimensional particle flow codes (PFC2D, PFC3D and XSite), respectively [11-13].

When the force is applied to the rock foundation, it reacts to this loading and will fail, settle down and deform depending on its mechanical properties. Indeed, this issue should be heeded in the construction of surface and sub-surface structures. In case deposition happens more than the initial forecast, it will destroy the structure. Further, the bearing capacity of its foundation is considered as the most essential factor bringing about the failure of a footing or a structure. Consequently, it is crucial to examine its bearing capacity in order to build an ideal foundation with reasonable stability. Notably, this is the indispensable part of the geotechnical engineering operations [14].

Remarkably, the penetration of a rigid body into a soft body has been also presented. In consequence, bearing capacity was presented based on the concept of plastic balance. Next, the formulations were also improved [15].

There is little literature deliberating the impacts of footing geometry and size on rock foundation settlement and bearing capacity. It should be pointed out that there are also some reports on soil bedding. In a dry sand experiment, the footing geometry impacted bearing capacity actually reflected a higher value in conic and pyramidal footings than in flat ones [16]. Notably, a series of experiments with square and strip footings placed on sand has been implemented. Considerably, it was determined that bearing capacity is increased as the footing dimensions get enhanced [17].

In this regard, rectangular footing on sand in the laboratory was dissected. Indeed, the final bearing capacity is enhanced as the footing area is grown [18]. The results are in consistent with the outcomes. Moreover, a physical experiment and finite element numerical model was practiced. Additionally, the bearing capacity of the foundation increased through scaling up the footings area [19].

The use of finite element numerical model in FLAC software has contributed to rise the bearing capacity by scaling up the footing width [20]. Researchers have previously verified that the scale significantly affects the bearing capacity. Moreover, the bearing capacity grown by proliferating the footing dimensions on a given foundation. The aim of this study is to investigate changes in bearing capacity in two states including a fixed footing area with different geometries and fixed footing geometry with increasing area.

The undesirable nature of soil and rock and the problems of experimental tests increase the tendency in the laboratory and onsite to seek alternative methods predicting the bearing capacity other than traditional computing techniques. In fact, more accurate results can be obtained [18]. Within recent decades, the use of numerical methods and models have been significantly developed in rock mechanics. Several researchers have been enthusiastic about this field [21-23]. Although some numerical models have not been able to completely solve the problem, it is possible to discover relationships among different parameters with the advent of sensitivity analysis methods

[24-26]. Some of these models are Boundary Element Method, Finite Element Method, Distinct Element Method and Finite Difference Method. There are also various models of materials in relevant software simplifying the analysis used by researchers to analyze the behavior of rocks by considering properties of discontinuity [27,28].

Linear failure and nonlinear resistance methods are inspected using Mohr-Coulomb [29]. The success of a foundation design relies on the precise estimation of its bearing capacity. To avoid onsite techniques, several methods have been developed by various researchers to estimate the bearing capacity. Despite this fact, it is crucial to improve more powerful predictive models [15]. After general shear failure, a triangle wedge is formed under the footing in a two-dimensional cross-section [30]. The purpose of this study is to deliberate the penetration of footing into the rock and subsequent foundation failure mechanism. It is noteworthy that the first comprehensive failure model in bearing capacity has been displayed [31].

Furthermore, it was specified that the internal angles of the triangle (critical angles) in soil are equal to ∅ [31]. It was calculated that the internal angles of a triangle in rock are equal to 45+∅/2 [30].

The assumption of small spacing of the fractures are mostly based on the existing equations determining the bearing capacity of rocks [32-38]. In some cases, the hypothesis of large spacing of the fractures are also practiced [33,35]. It is noteworthy that all these methods can only be employed when a general shear failure happens. If there is a punching failure, these methods are not properly accurate. Table 1 divulges the basic and primary formula of bearing capacity.

2- NUMERICAL MODEL

2-1- Particle Flow Code and PFC3D Programming

To make the numerical model, the particle flow code (PFC) was used in PFC3D software (Version 5.00.27). The PFC was first released in 1994. In fact, it is an advanced, fast, extremely versatile, commercial and multi-physics simulation software for engineers and scientists by means of the Distinct Element Method (DEM). Peter Cundall pioneered the DEM research and development. It has been nearly half of a century that PFC has been considered. PFC efficiently contributes the performance of industrial standards, ease of use, accuracy, and versatility for manufacturing, mining, geotechnical, earth sciences, pharmaceuticals, and packaging simulations.

2-2- Material and Properties

The grains used for foundation modeling were in dimensions of 4.75-12.5 mm like the fine gravel of Jalilabad zone in the east of Tehran, Iran. The behavioral model utilized in PFC3D was the parallel bond model. The mechanical properties were measured the same as the granite sample for the foundation. Additionally, all numerical experiments were performed thereon. The grain-

Table 1. Basic and primary formula of bearing capacity

Terzaghi (1943)	$q_u = cN_c + qN_q + \frac{1}{2}\gamma BN_\gamma$ N_c , N_q , N_γ= bearing capacity factors B = width of the footing c = unit cohesion q= effective stress at the level of the bottom of the foundation γ =unit weight
Meyerhof (1963)	$q_u = c\lambda_{cs}\lambda_{cd}\lambda_{ci}N_c + q\lambda_{qs}\lambda_{qd}\lambda_{qi}N_q + \frac{1}{2}\gamma B\lambda_{\gamma s}\lambda_{\gamma d}\lambda_{\gamma i}N_\gamma$ $\lambda_{cs}, \lambda_{qs}, \lambda_{\gamma s}$ = shape factors λ_{cd} , λ_{qd} , $\lambda_{\gamma d}$ =depth factors λ_{ci} , λ_{qi} , $\lambda_{\gamma i}$ = load inclination factors

size distribution diagram is indicated in PFC3D (Figure 1). Table 2 illustrates the specifications dealt with the foundation in a numerical model.

2-3- Micro- specifications

Micro- specifications of grains

E_C, $\frac{k_n}{k_s}$, μ

Micro specifications of cement

$\overline{E_c}$, $\bar{\lambda}$, $\frac{\bar{k}_n}{\bar{k}_s}$, $\bar{\sigma}_c$, $\bar{\tau}_c$

Where:

E_C and $\overline{E_c}$ are the elasticity modulus of grains and cement, the ratios of $\frac{k_n}{k_s}$ and $\frac{\bar{k}_n}{\bar{k}_s}$ are considered as the normal hardness ratio to the sheer ratio of grains and cement, respectively; $\bar{\lambda}$ is the parallel bond radius increase coefficient, μ is the friction coefficient of grains, $\bar{\sigma}_c$ and $\bar{\tau}_c$ are represent the tensile strength and the shear strength of parallel bonding, correspondingly.

2-4- Establishment of Model Geometry

In the current study, the specimens were in sizes of 700 mm (L), 400 mm (H), and 400 mm (D) filled by grains up to 350 mm. The numerical model is demonstrated in Figure 2. For this purpose, two series of footings were used with different quadratic, rectangular and circular geometries. Table 3 shows the dimensions and geometries of the footings.

3- RESULTS AND DISCUSSION

3-1- Effect of Footing Geometry

Figure 3 displays the displacement-force diagrams for different footing geometries in a total area of 64 cm^2. After the footing penetration

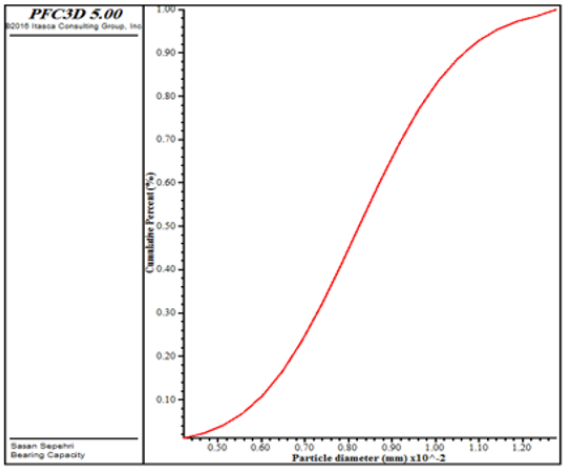

Figure 1. Grain- size distribution diagram in PFC3D

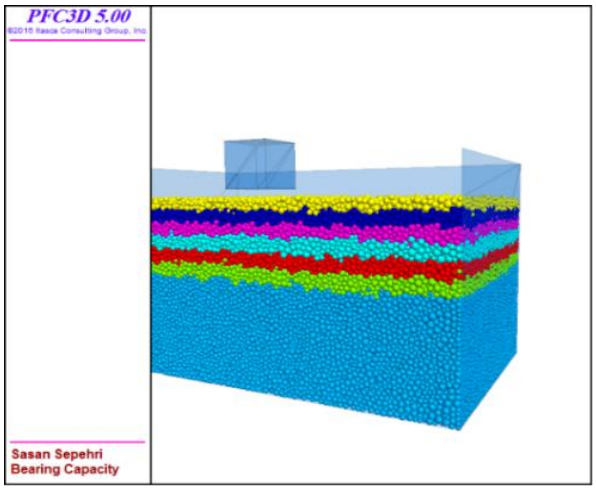

Figure 2. Three-dimensional numerical model (164000 particles)

Table 2. Material properties of rock

Row	Parameters	Unit	Value
1	Uniaxial compressive strength	MPa	99
2	Cohesion	MPa	16.5
3	Angle of friction	Deg.	50
4	Normal and Shear Stiffness	-	1e8
5	Density	Kg/m^3	2460

Table 3. Dimension and geometry of the designed foundations of numerical model

No.	Area (cm^2)	Geometry	Dimension (cm)
1	64	Square	8×8
2	64	Rectangle	7×9.14
3	64	Circle	R 4.51
4	49	Square	7×7
5	49	Rectangle	6×8.16
6	49	Circle	R 3.95

of 1.2 cm, a shear failure was detected in the foundation. The displacement-force diagram completely returned and referred to general shear failure [39]. After observing several experiments and monitoring diagrams, it was concluded that the displacement-force diagram consists of three parts before failure point. As shown in Figure 3, Section A is associated with the closure of empty spaces inside the rock and the release of small cracks. The footing movement will face with more rock resistance in the first stage of loading as the wedge does not form under the footing. Henceforth, the slope is low in the displacement-force diagram in Section A (Figure 3). As loading continues in B region, a wedge is formed with a semicircular tip (the slope is increased in this section). Furthermore, it facilitates footing movement in the rock. Finally, the wedge region is completed in Section C (Part 3 of displacement-force diagram) with the formation of a sharpened tip. This occurs when grains are detached from their places and positioned in such a way to form a complete wedge in which there is the highest penetration rate of the footing into the rock. Figure 3 exhibits the displacement-force diagram of the rock.

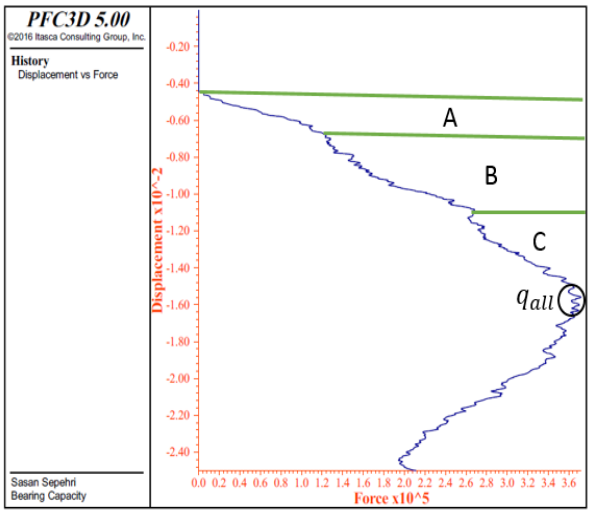

Figure 3. The displacement - force diagram for a square footing of 68 cm^2 area

Sections A, B and C (Figure 4) illustrate the displacement-force diagrams for rectangular and circular footings in an area of 68 cm^2.

According to Figure 5, the distribution of uplift is not uniform in different footing geometries. Besides, it takes different forms. For a square footing, the uplift will be mostly distributed in the center. Hence, the least distribution is taken place in the corners. In a rectangular footing, the sides are stretched to form a rhombus. In a circular footing, the uplift is formed as a circular ring around the foundation. This issue is generally subjected to changes relying on the distribution of grains for

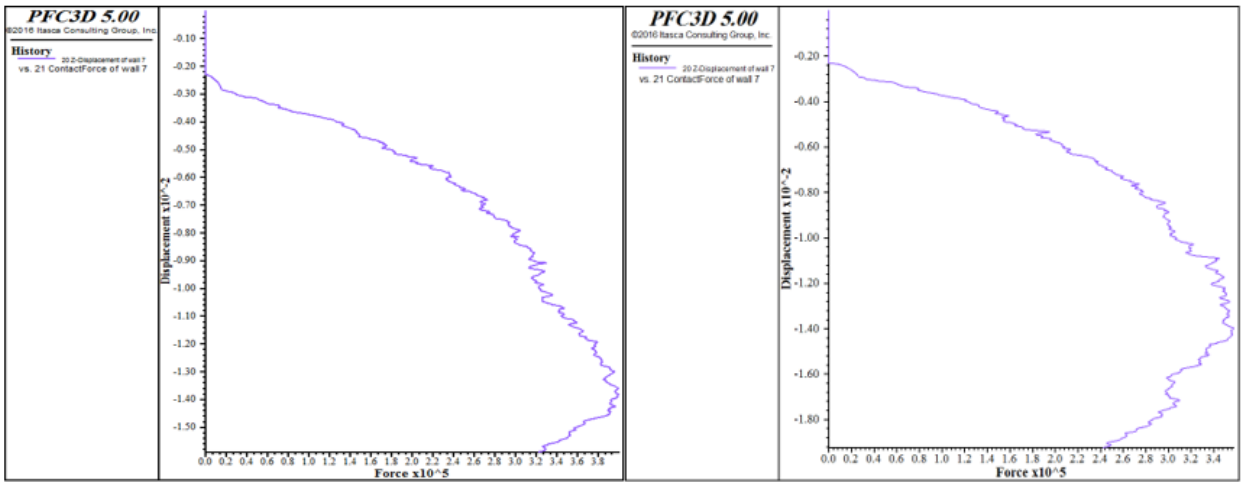

(A) **(B)**

Figure 4. The displacement - force diagram for a footing of 68 cm^2 area. A) The displacement - force diagram for a rectangular footing on dimensions of 9.14 × 7 cm. B) The displacement - force diagram for circular footing on radius of 4.51 cm

different footing geometries. Sometimes, it obeys the rules in which the grains form the rock bedding.

Conclusively, the bearing capacity would be higher in a circular footing than those of other footings. Besides, the bearing capacity of a square foundation will be greater than a rectangular foundation. The results obtained from numerical experiments are shown in Table 4.

As previously investigated by researchers, the bearing capacity gets increased as the footing size is accelerated. So far, this issue has been proved for all three quadratics, rectangular and circular footings using the particle flow theory. However, the highest rate of bearing capacity would be recorded for circular, quadratic and rectangular footings, respectively. From another point of view, changing the footing geometry does not remarkably influence the amount of settlement. Accordingly, an overall failure will occur when the footing reaches a certain depth which will not be affected by the footing geometry. Nevertheless, an increase in the footing area will not only increase the bearing capacity, but also will deepen the overall failure. Henceforward, there are two mechanisms: one is associated with the area where the settlement depth and bearing capacity will be increased and the other is related to the footing geometry in which only the bearing capacity is raised. Figure 6 elucidates the bearing capacity

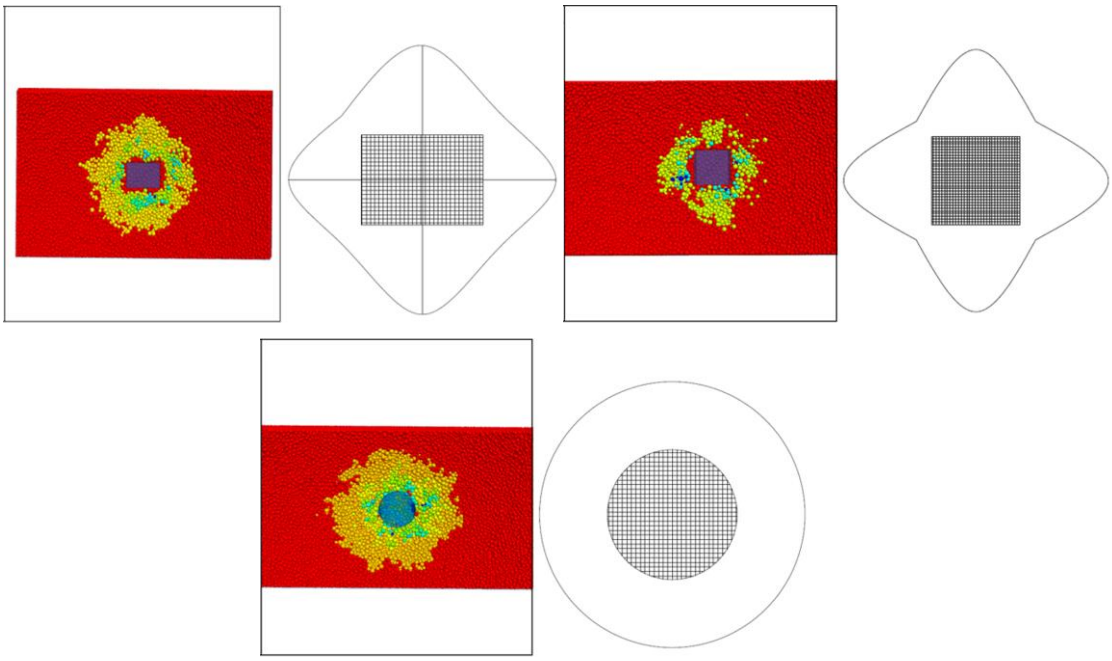

Figure 5. Uplift geometry around square, rectangular and circular footings

Table 4. Numerical tests results

No.	Geometry	Area (cm^2)	Dimension (cm)	Force (kN)	Settlement (cm)
1	Square	64	8×8	370	1.12
2	Rectangle	64	7×9.14	350	1.14
3	Circle	64	R 4.51	400	1.13
4	Square	49	7×7	272	0.93
5	Rectangle	49	6×8.16	264	1.02
6	Circle	49	R 3.95	320	0.99

diagrams and failure geometry for different types of footings with an area of 49 cm^2. The images are taken at a constant time and a definite section, whereas different shapes of the failure and the bearing capacity diagram indicate that they are influenced by the footing geometry.

The failure geometry obeys the bedding grain size. Also, the failure geometry in the right side is not similar to the left one in a 7×7 cm footing (Figure 6). This asymmetry is decreased in the rectangular footing and becomes more symmetric in the circular one.

3-2- Failure Mechanism

The active Rankin state formed under the footing theoretically makes a triangle in two dimensions and a wedge in three dimensions. Moreover, the internal angle of the two sides of the triangle are congruent if the foundation is composed of heterogeneous grain-size distribution. These angles will be affected by this gradient and the triangle shape will be asymmetric.

The effect of grain-size distribution on the shape of failure was demonstrated and proved in this study. An asymmetric wedge is formed according to the position and size of grains. As shown in Figure 7, this wedge is verified in the form of an asymmetric triangle in a two-dimensional cross section. The vertex of the triangle is not tanged to the central axis of the footing making an asymmetric distribution of force under the footing, which will explain tilting the structure. Tilting occurs in many surface structures. This brings about the conclusion that one of its most significant factors is heterogeneity of the bedding.

If the displacement-force diagram passes through Step A (Figure 3), the elastic deformations are finished, the plastic deformations get started, the cracks are propagated in the foundation and the wedge begins to be formed. In case the grain-size distribution is not homogeneous under the footing, an asymmetric wedge is automatically formed. In consequence, the structure is tilted. Both the torque force and force withdrawal from the center will increase the failure velocity and penetration of the footing. In due course, it makes the structure to fall onto one side.

Figure 7 clarifies a cross section of a wedge in

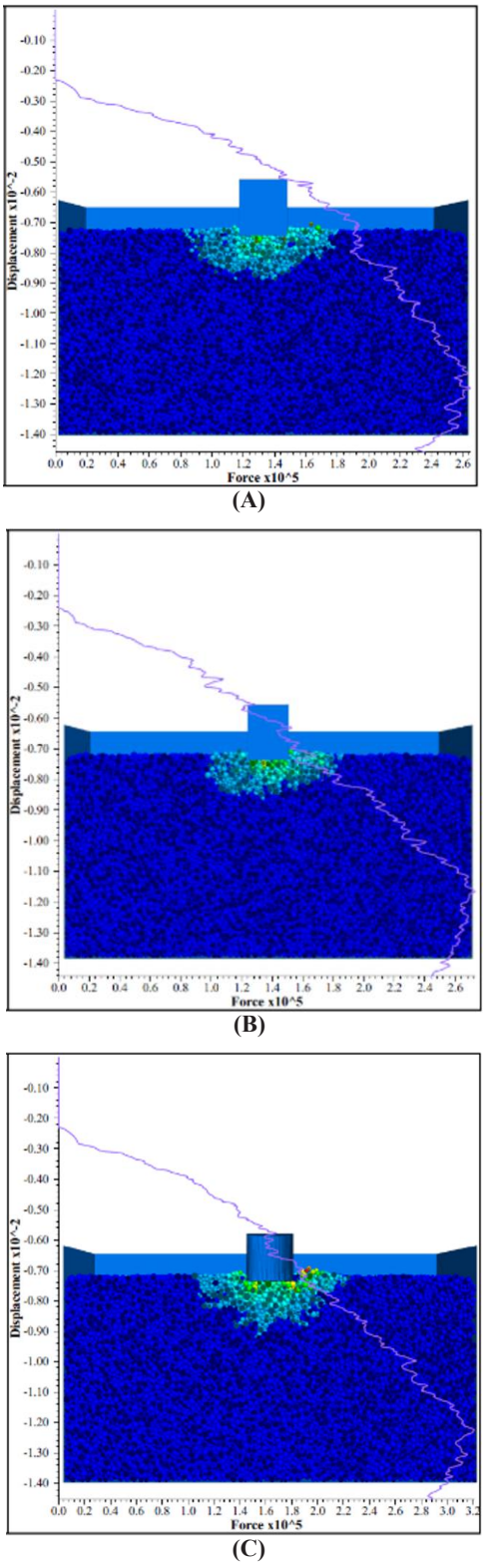

Figure 6 The displacement - force diagram and failure geometry for a footing of 49 cm^2, A) Dimension of 7 × 7 cm, B) Dimension of 8.16 cm, C) Radius of 3.95 cm

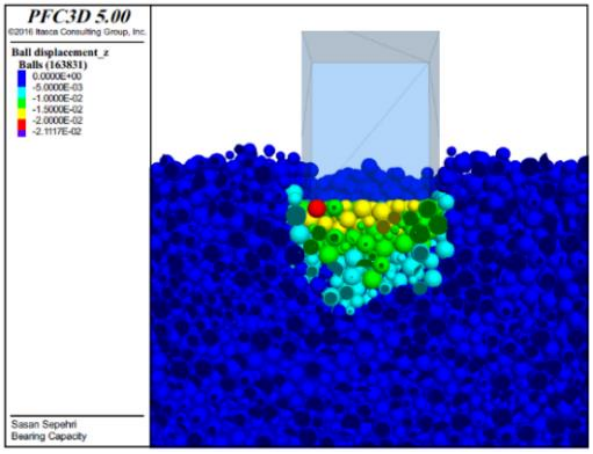

Figure 7. Failure triangle under the footing with 8 × 8 cm dimension (Active Rankine state)

the form of triangle angles smaller and greater than ∅. Nonetheless, the angles are close to ∅ in this study. If the effect of the foundation heterogeneity on the angles is eliminated, it may be determined that the internal angle of the triangle in the rock is equal to ∅.

Asymmetries of the triangular area create an asymmetric uplift around the foundation. Moreover, the failure shape in the zone of radial shear and passive Rankin will be different on each side of footing. The depth of defect is reduced and the radius of the impact becomes longer in a place with less inner angle. Over the entire path, the deflection will be longer and the soil drainage inclination underlying the footing. As the internal angle of the triangle gets greater, the depth of failure will be proliferated. Thus, the failure impact radius becomes shorter. In the whole path, the failure will be shortened and the soil drainage inclination in the foundation will be escalated from the same side (Figure 8).

According to Figure 7, the maximum displacement is equal to 2.1E-2 meters. The blue grains are located in this displacement range on the left side of the footing. Similarly, a comparison of displacements on the left and right sides of the footing (Figure 8) clearly indicates that the greatest displacement is 1.57E-2 meters. This occurred on the left side of the footing. These observations determine that the grains on the left side of the footing have more displacement than the ones on the right side.

This asymmetry in the triangle disappears after further penetration and passing the failure phase. As a cube box (8 × 8 cm) in a downward movement at fixed and constant speed was practiced as a footing, the grains underlying the footing displaced and created a symmetric triangle. However, this phenomenon will tilt the structure in nature.

With further penetration of footing into the rock and symmetry of the triangle under the footing, the zone of radial shear and passive Rankin will also be symmetric. Lastly, a symmetrical failure is obtained similar to that of Terzaghi's (Figure 9). The general shear failure ends after the footing is penetrated up to 2.14 cm.

As shown in Figure 10, the displacements were filtered in the positive and negative directions of X-axis (the length of the test box) and reached the grains with the highest displacement in the X -axis. This will make two zones: the one on the right and the other on the left side of the triangle below the footing, which are similar to the radial shear zone in the failure mechanism.

Figure 11 displays that displacements in the positive direction of the Z-axis were filtered (means in the direction of the test box height) and reached the grains with the highest displacement in the positive direction of the Z-axis. This will create two zones: one on the right and the other on the left side of the footing, which are similar to the passive Rankin zone in Terzaghi failure mechanism.

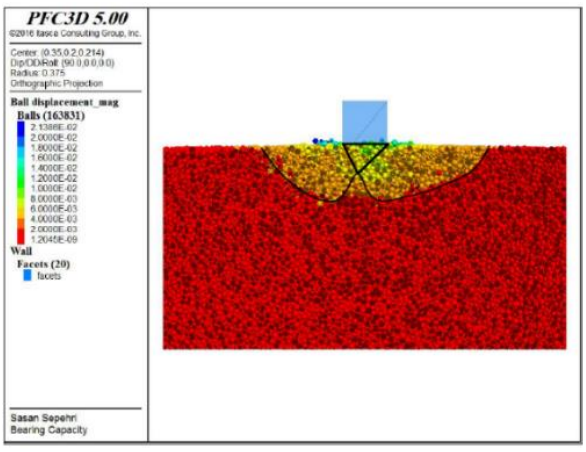

Figure 8. The geometry of failure when general shear starts

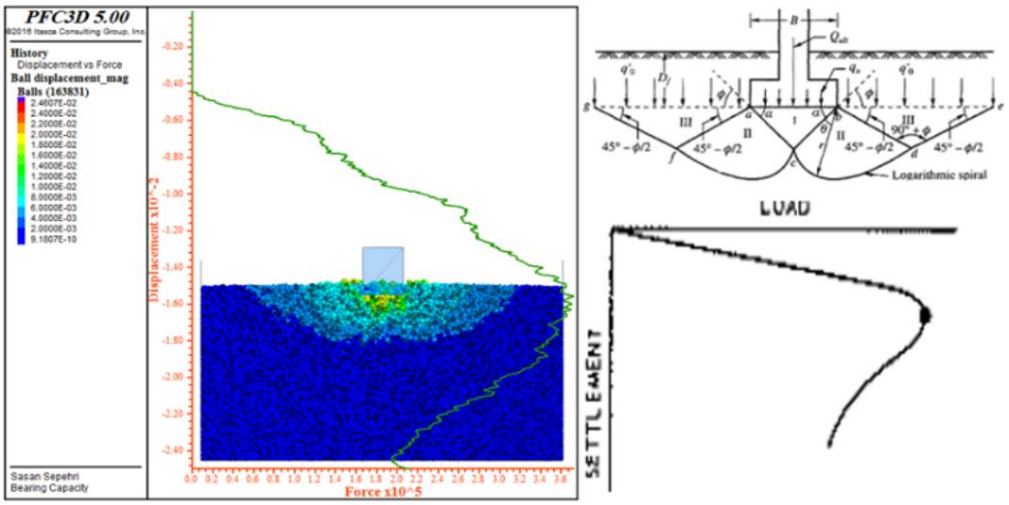

Figure 9. End of general shear failure after formation of symmetric triangle [31,39]

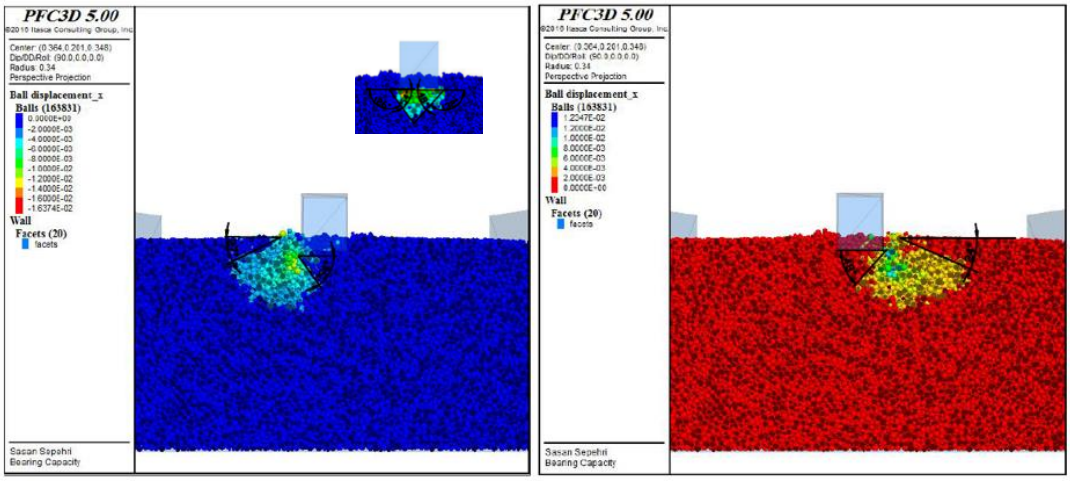

Figure 10. Grains with positive and negative horizontal motion in rock (Zone of radial shear)

These images were put on each other to determine the failure mechanism. As shown in Figure 12, there will be generally four areas for each foundation

side. Region A is the half of the failure triangle underlying the footing. The grains move downward in this region. Region B is related to the grains moving almost horizontally and in a sheered manner. Region C is connected to the grains in a vertical upward movement and cause the uplift phenomenon. At the point shared by regions B and C, there is an extra region called Region D in which horizontal and vertical displacements simultaneously occur. This area has with the doughiest state and the most tension.

4- CONCLUSIONS

In the light of most important results, the following conclusions can be drawn:

1) The displacement-force diagram includes three areas before the failure point. Area A is associated with the closure of empty spaces inside the rock and the release of small cracks. Region B is an incomplete triangle with a round vertex formed underlying the footing. Region C is where

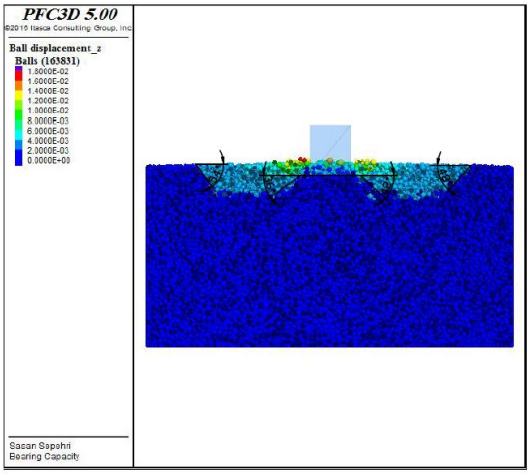

Figure 11. Grains with upward motion in the rock (passive Rankin zone)

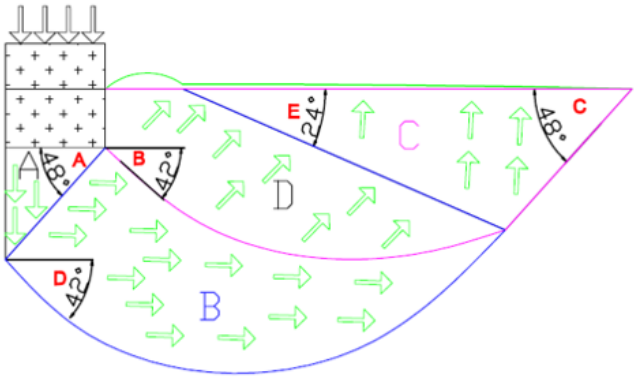

Figure 12. Failure shape in the rock foundation (Region B and C are shown by blue and purple boundaries respectively)

the triangle is completely formed in which the penetration of the footing will be at the highest speed.

2) The uplift appears the same in any particular geometry. In a square footing, the uplift is mostly expanded in the center of the foundation. Notably, the least expansion is figured out in the corners. It forms a rhombus in a rectangular footing and a circle in a circular base. In different footings, this issue relies on changes based on the distribution of grains and their heterogeneity.

3) Two mechanisms have been found in bearing capacity and settlement. The first mechanism is associated with the footing area in which the depth and bearing capacity will be increased, accordingly. The second one is related to the footing geometry and the load capacity will be only changed when it is altered at a constant area.

4) If the underlying footing is not homogeneous, an asymmetric wedge zone is automatically formed. Both the torque force and force withdrawal from the center will increase the failure velocity and penetration of the footing. In due course, it makes the structure to fall onto one side.

5) The failure area is divided into four zones. Zone A, which is a wedge failure area, lies in two dimensions of a triangular shape. The pressure that area A exerts on the bed will subject the grains to be sheered in zone B. Grain shearing in zone B affects the grains to move upward in zone C. Zone D will be located between B and C, where the grain upwardly moves. Holistically, it is the tension stress binding the region into two regions B and C.

6) If it is assumed that the internal angle of the triangle is equal to ∅, a discontinuity plate will be formed with a slope ∅ on each side. The pressure applied by zone A to the substrate will cause the grains to be sheered in zone B. The sheered grains of zone B lead the particles to move upward in zone C and eventually move to the ground on a fracture plane under the angle ∅. The point shared by zones B and C is called zone D, where the grains obliquely move upward. In fact, it is the tension stress binding the region into two regions B and C. The uplift is decreased as it gets far from the footing. As a result, the highest uplift will be taken place near the footing.

5- REFRENCES

[1] Hosseini, N. H., and Fatehi, M. M. (2007). *"A semi-infinite higher-order displacement discontinuity method and its application to the quasistatic analysis of radial cracks produced by blasting"*. Journal of Mechanics of Materials and Structures, 2(3): 439-458.

[2] Fatehi, M. M. (2013). *"On the use of power series solution method in the crack analysis of brittle materials by indirect boundary element method"*. Engineering Fracture Mechanics, 98: 365-382.

[3] Fatehi, M. M. (2014). *"Numerical analysis of quasi-*

static crack branching in brittle solids by a modified displacement discontinuity method". International Journal of Solids and Structures, 51(9): 1716-1736.

[4] Fatehi, M. M. (2015). *"Simulation of crack coalescence mechanism underneath single and double disc cutters by higher order displacement discontinuity method"*. Journal of Central South University, 22(3): 1045-1054.

[5] Haeri, H., Khaloo, A., and Fatehi, M. M. (2015). *"Experimental and numerical simulation of the microcrack coalescence mechanism in rock-like materials"*. Strength of Materials, 47(5): 740-754.

[6] Abdollahipour, A., Fatehi, M. M., Bafghi, A. Y., and Gholamnejad, J. (2016). *"Time-dependent crack propagation in a poroelastic medium using a fully coupled hydromechanical displacement discontinuity method"*. International Journal of Fracture, 199(1): 71-87.

[7] Lak, M., Fatehi, M. M., Bafghi, A. Y., and Abdollahipour, A. (2019). *"A Coupled Finite Difference-Boundary Element Method for modeling the propagation of explosion-induced radial cracks around a well bore"*. Journal of Natural Gas Science and Engineering, 64(1): 41-51.

[8] Cundall, P. A., and Strack, O. D. L. (1979). *"A discrete numerical model for granular assemblies"*. Geotechnique, 29(1): 47-65.

[9] Cundall, P. A. (1987). *"Distinct Element Models of Rock and Soil Structure"*. In Brown E. T. (ed.), Analytical and Computational Methods in Engineering Rock Mechanics, London: Allen & Unwin, Ch. 4, 129-163.

[10] Itasca (1999). PFC2D (Particle Flow Code in 2 Dimensions) User's Guide, Itasca Consulting Group, Inc., Minneapolis.

[11] Sarfarazi, V., Haeri, H., and Fatehi, M. M. (2019). *"Numerical simulation of the effect of bedding layer on the tensile failure mechanism of rock using PFC2D"*. Structural Engineering and Mechanics, 69(1): 43-50.

[12] Haeri, H., Sarfarazi, V., Zhu, Z., Marji, M. F., and Masoumi, A. (2019). *"Investigation of shear behavior of soil-concrete interface"*. Smart Structures and Systems, 23(1): 81-90.

[13] Bakhshi, E., Rasouli, V., Ghorbani, A., Fatehi, M. M., and Damjanac, B. (2019). *"Numerical Simulations of Lab-Scale Hydraulic Fracture and Natural Interface Interaction"*. Rock Mechanics and Rock Engineering, 52(5): 1315-1337.

[14] Baazouzi, M. (2016). *"2d numerical analysis of shallow foundation rested near slope under inclined loading"*. Elsevier, Procedia Engineering, 143: 623-634. DOI: 10.1016/j.proeng.2016.06.086.

[15] Tajeri, Sh. (2015). *"Indirect estimation of the ultimate bearing capacity of shallow foundations resting on rock masses"*. International Journal of Rock Mechanics & Mining Sciences, Elsevier Ltd., 107–117. DOI: 10.1016/j.ijrmms.2015.09.015.

[16] Fernando, N. (2011). *"The Experimental Investigation of Failure Mechanism and Bearing Capacity of Different Types of Shallow Foundation"*. Civil Engineering Research for Industry, Department of Civil Engineering, University of Moratuwa.

[17] Castelli, F., and Lentini, V. (2015). *"Evaluation of the Bearing Capacity of Footings on Slopes"*. International Journal of Physical Modelling in Geotechnics, 15(3): 165-168. DOI: 10.1680/jphmg.14.00038.

[18] Dixit, M. S. (2013). *"Experimental Estimate of Ultimate Bearing Capacity and Settlement for Rectangular Footings"*. International Journal of Civil Engineering and Technology (IJCIET), 4(2): 337-345.

[19] Mohamed, I. R., and Mohamed, H. H. (2015). *"Bearing Capacity of Sand Overlying Clay – Strip Footing"*. International Journal of Science and Research (IJSR), 4(2): NOV151560.

[20] Acharyya, R., and Dey, R. (2017). *"Finite Element Investigation of the Bearing Capacity of Square Footings Resting on Sloping Ground"*. Springer, Indian National Academy of Engineering, 97-10. DOI: 10.1007/s41403-017-0028-6.

[21] Jan, I. I. (1996). *"Short descriptions of UDEC and 3DEC"*. Developments in Geotechnical Engineering, vol. 79: 523-528. DOI: 10.1016/S0165-1250(96)80041-1.

[22] Waltham, A. C. (2004). *"Bearing capacity of rock over mined cavities in Nottingham"*. Engineering Geology, 75(1): 15-31. DOI: 10.1016/j.enggeo.2004.04.006.

[23] Wang, J. T. (2011). *"Investigation of damping in arch dam-water-foundation rock system of Mauvoisin arch dam"*. Soil Dynamics and Earthquake Engineering, 31(1): 33-44. DOI: 10.1016/j.soildyn.2010.08.002.

[24] Souley, M., and Homand, F. (1996). *"Stability of jointed rock masses evaluated by UDEC with an extended Saeb-Amadei constitutive law"*. International Journal of Rock Mechanics and Mining Sciences & Geomechanics, 33(3): 233-244. DOI: 10.1016/0148-9062(95)00063-1.

[25] Zhou, H. Z., Zheng, G., Yu, X. X., Zhang, T. Q., and Liu, J. J. (2018). *"Bearing capacity and failure mechanism of ground improved by deep mixed columns"*. Journal of Zhejiang University Science A, 19(4): 266-276. DOI: 10.1631/jzus.A1700517.

[26] Bayraktar, A., Sevim, B., and Altunişik, A. C. (2011). *"Finite element model updating effects on nonlinear seismic response of arch dam–reservoir–foundation systems"*. Finite Elements in Analysis and Design, 47(2): 85-97. DOI: 10.1016/j.finel.2010.09.005.

[27] Eduardo, M., Bretas, P., and Jose, V. (2012). *"3D stability analysis of gravity dams on sloped rock foundations using the limit equilibrium method"*. Computers and Geotechnics, 44: 147-156. DOI: 10.1016/j.compgeo.2012.04.006.

[28] Lin, Y., Zhu, D., Deng, Q., and He, Q. (2012). *"Collapse Analysis of Jointed Rock Slope Based on UDEC Software and Practical Seismic Load"*. Procedia Engineering, 31: 441-446. DOI: 10.1016/j.proeng.2012.01.1049.

[29] Kate, J. M., and Nigam, P. K. (2008). *"Comparative study of bearing capacity estimates of a footing on jointed rock mass by different approaches"*. 12th Conference of IACMAG, 3133-3139.

[30] Meyerhof, G. G. (1953). *"Bearing capacity of concrete and rock"*. Magazine of Concrete, April. DOI: 10.1680/macr.1953.4.12.107.

[31] Terzaghi, K. (1943). *"Theoretical soil mechanics"*. 42-65.

[32] Merifield, R. S., Lyamin, A. V., and Sloan, S. W. (2006). *"Limit analysis solutions for the bearing capacity of rock masses using the generalised Hoek–Brown criterion"*. International Journal of Rock Mechanics and Mining Sciences, 43: 920-937. DOI: 10.1016/j.ijrmms.2006.02.001.

[33] Prakoso, W. A., and Kulhawy, F. H. (2004). *"Bearing Capacity of Strip Footings on Jointed Rock Masses"*. Journal of Geotechnical & Geoenvironmental Engineering, 130(12): 1347-1349. DOI: 10.1061/10900241130.

[34] Saada, Z., Maghous, S., and Garnier, D. (2008). *"Bearing capacity of shallow foundations on rocks obeying a modified Hoek–Brown failure criterion"*. Computers and Geotechnics, 35(2): 144- 154. DOI: 10.1016/j.compgeo.20.06.003.

[35] Serrano, A., and Olalla, C. (1998). *"Ultimate bearing capacity of an anisotropic discontinuous rock mass, Part I: Basic modes of failure"*. International Journal of Rock Mechanics and Mining Sciences, 35(3): 301- 324. DOI: 10.1016/S0148-9062(97)00337-9.

[36] Singh, M., and Rao, K. S. (2005). *"Bearing Capacity of Shallow Foundations in Anisotropic NonHoek–Brown Rock Masses"*. Journal of Geotechnical & Geoenvironmental Engineering, 131(8): 1014-1023. DOI: 10.1061/(ASCE)1090-0241.

[37] Sutcliffe, D. J., Yu, H. S., and Sloan, S. W. (2004). *"Lower bound solutions for bearing capacity of jointed rock"*. Computers and Geotechnics, 31: 23-36. DOI: 10.1016/j.compgeo.2003.11.001.

[38] Yang, X. L., and Yin, J. H. (2005). *"Upper bound solution for ultimate bearing capacity with a modified Hoek-Brown failure criterion"*. International Journal of Rock Mechanics and Mining Sciences, 42: 550- 560. DOI: 10.1016/j.ijrmms.2005.03.002.

[39] Vesic, A. S. (1973). *"Analysis of Ultimate Loads of Shallow Foundations"*. Journal of the Soil Mechanics and Foundations Division, 99(1): 45-73. DOI: 10.1016/0148-9062(74)90598-1.